# Density Functional Theory Calculations and Analysis of Reaction Pathways for Reduction of Nitric Oxide by Hydrogen on Pt(111)

Carrie A. Farberow, James A. Dumesic,* and Manos Mavrikakis*

Department of Chemical and Biological Engineering, University of Wisconsin, Madison, Wisconsin 53706, United States

ABSTRACT: Reaction pathways are explored for low temperature (e.g., 400 K) reduction of nitric oxide by hydrogen on Pt(111). First-principles electronic structure calculations based on periodic, self-consistent density functional theory (DFT-GGA, PW91) are employed to obtain thermodynamic and kinetic parameters for proposed reaction schemes on Pt(111). The surface of Pt(111) during NO reduction by H_2 at low temperatures is predicted to operate at a high NO coverage, and this environment is explicitly taken into account in the DFT calculations. Maximum rate analyses are performed to assess the most likely reaction mechanisms leading to formation of N_2O, the major product observed experimentally at low temperatures. The results of these analyses suggest that the reaction most likely proceeds via the addition of at least two H atoms to adsorbed NO, followed by cleavage of the N−O bond.

KEYWORDS: catalysis, nitric oxide reduction, platinum, density functional theory, maximum rate analysis, reaction mechanism
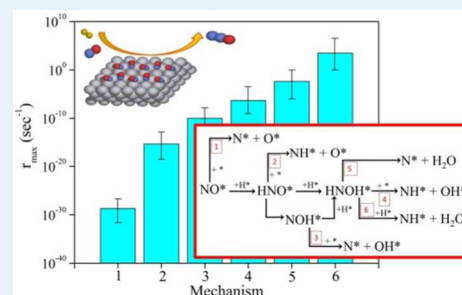
INTRODUCTION

The catalytic conversion of nitric oxide, an unwanted byproduct of the combustion of hydrocarbons in air, to N_2 is of fundamental and practical importance.[1−5] Platinum catalysts are active for the reduction of NO by H_2, but at low temperatures these catalysts demonstrate low selectivity toward N_2 and unfavorable production of side-products, namely, N_2O and NH_3.[6−8] The relative selectivity to N_2O versus NH_3 is, among other factors, dependent on the NO to H_2 ratio. Thus, at high NO to H_2 ratios, improved selectivity for NO reduction by H_2 requires identification of materials for which the reaction kinetics favor N_2 formation over N_2O. Previous studies of NO reduction by H_2 on Pt catalysts have generally assumed that the reaction mechanism begins with N−O activation by (i) direct dissociation of NO or (ii) hydrogenation followed by N−O bond cleavage.[7,9,10]

$$NO* + * \rightarrow N* + O* \qquad (i)$$

$$NO* + H* \rightarrow NOH* + * \qquad (ii)$$

$$NOH* + * \rightarrow N* + OH*$$
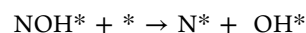
The major products are then formed through subsequent hydrogenation or N−N bond formation steps.

In this work, we conducted a theoretical investigation, using electronic structure calculations based on planewave density functional theory (DFT-GGA), to probe the role of hydrogen in N−O activation. We begin this study by predicting the surface coverage of nitric oxide under low-temperature reaction conditions and by directly investigating the impact that NO coverage has on the reaction energetics. In addition to the H-assisted pathway for N−O activation via NOH* suggested in the literature, we consider the possibility of an alternative

HNO* intermediate and the addition of extra H* to NO* prior to N−O bond cleavage.

Typically, to rigorously probe the mechanistic pathway of a reaction under realistic conditions from first-principles calculations, it is useful to construct a microkinetic model to describe the experimental kinetic data.[11,12] Because of the time and effort required by this approach, we suggest here a simplified approach, denoted as maximum rate analysis, to identify the most likely pathway(s) in complicated reaction schemes, making it possible to reduce the number of steps considered in more detailed kinetic models. We illustrate this approach to address various pathways for low-temperature NO reduction by H_2 on Pt(111).

METHODS

Density functional theory calculations were performed using the Vienna Ab initio Simulation Package (VASP).[13,14] The exchange-correlation functional was described by the generalized gradient approximation (GGA-PW91).[15] The electron−ion interactions were described by projector augmented wave (PAW) potentials.[16,17] The electron wave function was expanded using plane waves with an energy cutoff of 400 eV.

The Pt(111) surface was modeled by a (2 × 2) unit cell, periodically repeated in a super cell geometry with successive four-layer slabs separated by six equivalent layers of vacuum. The bottom two layers of the metal slab were fixed in their bulk truncated positions, whereas the top two layers were allowed to relax. The surface Brillouin zone was sampled with a 6 × 6 × 1 Monkhorst−Pack k point grid.[18] Adsorption was allowed on

only one of the two exposed metal surfaces per slab, and the electrostatic potential was adjusted accordingly.[19,20] Structures were fully relaxed until the Hellmann–Feynman forces acting on the atoms were smaller than 0.05 eV/Å. The optimized lattice parameter of bulk Pt was calculated to be 3.98 Å, in agreement with the experimental value of 3.92 Å.[21]

The reported binding energies (BE) of adsorbates were calculated with respect to a clean relaxed Pt(111) slab ($E_{Pt(111)}$) and the respective adsorbate in the gas-phase (E_{gas}).

$$BE = E_{total} - E_{Pt(111)} - E_{gas}$$

where E_{total} is the total energy of the slab with the adsorbate on it. Convergence of the total energy with respect to the k point set, energy cutoff and the number of metal layers included, was confirmed. Minimum energy pathways and activation energy barriers for all elementary steps were calculated using the climbing-image nudged elastic band (CI-NEB) method.[22,23] At least seven intermediate images were interpolated between reactant and product states for each elementary step. The transition state of the minimum energy pathway for each elementary step was confirmed by vibrational frequency calculations yielding a single imaginary frequency along the reaction coordinate.[24]

The phase diagram for NO/Pt(111) was generated by calculating the grand potential (Ω) at discrete coverages of 0.25, 0.50, 0.75, and 1.00 monolayer (ML). The grand potential is defined as

$$\Omega = E_{NO/Pt} - E_{Pt} - N_{NO}*\mu_{NO} - T*S$$

where $E_{NO/Pt}$ is the total energy of the Pt(111) slab with N_{NO} NO molecules adsorbed, E_{Pt} is the total energy of the clean Pt(111) slab, μ_{NO} is the chemical potential of NO, T is the absolute temperature, and S is the entropy of the Pt(111) slab with N_{NO} NO molecules adsorbed. The chemical potential of NO was calculated by

$$\mu_{NO}' = k_B*T*\ln\frac{P}{P^0}$$

$$\mu_{NO} = \mu_{NO}' + E_{NO} - T*S_{NO}$$

where k_B is the Boltzmann constant, P is the NO pressure, P^0 is the reference pressure of 1 atm, E_{NO} is the total energy of NO in the gas phase, and S_{NO} is the entropy of gas-phase NO.

To model a high NO-coverage environment in the DFT calculations, we completed DFT calculations which included 0.5 ML NO "spectators" in the periodic unit cell. For the 2 × 2 unit cell used in this study, 0.5 ML NO spectators corresponds to two NO adsorbates in addition to the adsorbate(s) studied for a thermochemistry calculation or participating in the elementary step for the respective CI-NEB calculation. The NO spectator species are relaxed during the calculation. The reported binding energies of adsorbates on Pt(111) with 0.5 ML coadsorbed NO spectators were calculated with respect to a relaxed Pt(111) slab with 0.5 ML adsorbed NO ($E_{0.5\ ML\ NO/Pt(111)}$) and the respective adsorbate in the gas phase (E_{gas}).

$$BE = E_{total} - E_{0.5\ ML\ NO/Pt(111)} - E_{gas}$$

where E_{total} is the total energy of the slab with the adsorbate and 0.5 ML coadsorbed NO. The calculations which include two NO spectator molecules will be referred to throughout the text as the "high-coverage" calculations. DFT calculations

completed on the clean Pt(111) surface will be referred to throughout the text as the "low-coverage" calculations.

■ RESULTS

NO Surface Coverage. The minimum energy configurations for NO adsorption at coverages of 0.25, 0.50, 0.75, and 1.00 ML on Pt(111), shown in Figure 1, are in agreement with
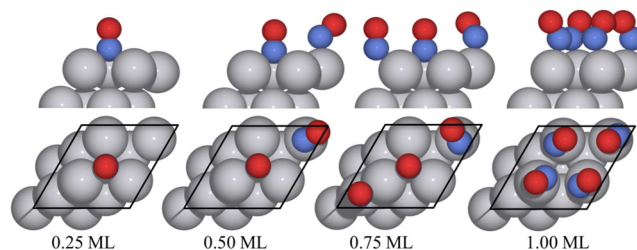
Figure 1. Minimum energy geometries for NO adsorption at varying coverages on the 2 × 2 unit cell of Pt(111); cross-section and top views shown in upper and lower panels, respectively. The periodic unit cell in the x and y direction is indicated by the black line. Red, blue, and gray spheres represent O, N, and Pt, respectively.

the preferred adsorption sites determined in high resolution X-ray photoelectron spectroscopy experiments conducted by Zhu et al.[25] At 0.25 ML coverage, NO occupies the fcc site, oriented perpendicular to the Pt(111) surface, with a binding energy of −1.88 eV. This behavior is in agreement with previous theoretical studies[26−28] as well as the experimentally determined binding energy of −1.65 eV found by Wartnaby et al. using single-crystal microcalorimetry on Pt(110).[29] The additional NO adsorbate present at 0.5 ML NO coverage occupies the top site and is oriented at an angle of 39.5° relative to the surface. The differential binding energy of the second NO molecule in the unit cell is −1.42 eV. A third NO molecule adsorbed in the unit cell, corresponding to a total NO coverage of 0.75 ML, occupies the hcp site with a binding energy of −1.05 eV. At 0.75 ML NO coverage, the NO adsorbed in the top site is tilted at an angle of 44.4° relative to the surface, whereas the NO molecules adsorbed in the hcp and fcc sites are oriented perpendicular to the surface. At 1 ML NO coverage, all adsorbed NO molecules occupy top sites and are oriented at angles of ∼59−60° relative to the surface. The differential binding energy of the fourth NO molecule (at a total of 1 ML NO coverage) is mildly endothermic (BE = 0.03 eV). The NO adsorption configurations and differential binding energies found in this study are consistent with previous theoretical studies reported in the literature.[30,31]

Phase diagrams for NO adsorption, derived from the DFT-calculated minimum energy states are shown in Figure 2 at varying NO coverage.[24,32] Figure 2a, depicting NO adsorption as a function of NO pressure at 400 K, shows that 0.75 ML NO is thermodynamically stable on Pt(111) at NO pressures up to 1 atm. The phase diagram for NO adsorption as a function of temperature at an NO pressure of 0.005 atm (Figure 2b) shows that 0.75 ML NO coverage remains the most thermodynamically stable state at temperatures from 300 to 1000 K. The choice of temperature and NO partial pressure in the phase diagrams are set on the basis of typical experimental conditions. The predicted coverage found from the phase diagram motivated the choice of two NO spectators for the high-coverage DFT calculations on Pt(111), because this corre-
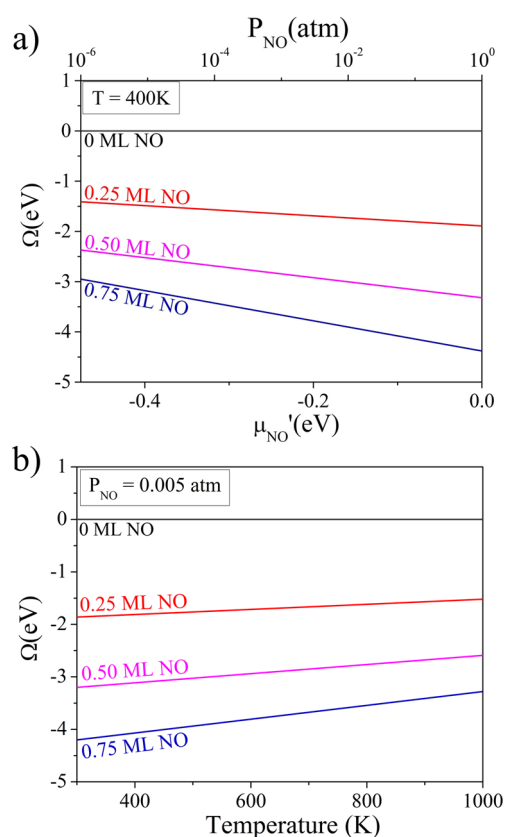
Figure 2. Phase diagram for NO coverage on Pt(111) (a) as a function of NO pressure at 400 K and (b) as a function of temperature at an NO pressure of 0.005 atm. The most stable state at a given pressure corresponds to the NO coverage with the most negative value for the grand potential, Ω.

sponds to a total NO coverage of 0.75 ML at the initial state for direct NO dissociation.

Adsorption. The results of the thermochemistry calculations at high (0.5 ML NO spectators) and low NO coverage are shown in Figure 3. Throughout the text, "*" refers to an empty surface site, and "A*" indicates adsorbed intermediate A. The DFT-calculated binding energies on clean Pt(111) are in agreement with previous work by Ford et al.[26] All adsorbates, excluding NH$_3$*, are destabilized by the 0.5 ML coadsorbed NO. NH$_3$ is characterized by very similar binding energy on the low-coverage and the high-coverage surface. The degree of destabilization of adsorbates is most significant for species that bind strongly to the surface (N*, NH*, O*) and least significant for the closed-shell adsorbates that are weakly bound to the surface (H$_2$O*, N$_2$*). The binding energy for N$_2$ is reduced from −0.12 eV on clean Pt(111) to 0 eV (does not adsorb) on the high-coverage surface. N$_2$O and molecular H$_2$ do not adsorb on the clean Pt(111) surface or the high-coverage surface. A majority of the adsorbates studied (nine of 14), which adsorb on the low and high-coverage surfaces, retain their low-coverage site preference on the high-coverage surface (Figure 3). The preferred adsorption site for H*, OH*, and HNNO* at low-coverage changes on the high-coverage surface. However, the difference in the stability of the sites at low coverage is less than 0.06 eV. HNO* prefers to adsorb at the br-top site on the low-coverage surface. In this configuration, the N in HNO* is coordinated to two Pt surface atoms at a bridge site, and the O in HNO* binds to one Pt atom at a top

site (Figure 3). In contrast, on the high-coverage surface, HNO* binds at a top site through its N atom. ONNOH* adsorbs through both N atoms on neighboring top sites (top-top) on the low-coverage surface, whereas on the high-coverage surface, it adsorbs through only one of its N atoms at a top site. In all systems, the spectator NO molecules occupy the remaining available fcc, hcp, and/or top sites, which maximize the distance between all of the coadsorbates in the unit cell studied.

Elementary Steps: Reaction Energies and Activation Energy Barriers. The activation energy barriers (E_A) and reaction energies (ΔE) of all elementary steps studied at high and low coverage are shown in Table 1.

H$_2$ + 2* → 2H*. The dissociative adsorption of H$_2$ is spontaneous on the clean surface but has an activation energy barrier of 0.65 eV on the high NO coverage surface. On the clean surface, the reaction is exothermic with a reaction energy of −0.87 eV, whereas on the high-coverage surface, the reaction is thermoneutral with a reaction energy of 0.08 eV. On the high coverage surface, the transition state lies above a Pt bridge site (Figure 4) and the H−H bond distance is 0.85 Å.

NO* + * → N* + O*. The NO coverage has the largest effect on the activation energy barrier for direct NO dissociation (NO* + * → N* + O*), where the barrier increases from 2.32 eV on the clean surface to 3.52 eV on the high-NO-coverage surface. These large activation energy barriers are in agreement with experimental studies showing that NO does not decompose on Pt(111) at low temperatures.[33,34] Direct NO dissociation is significantly more endothermic on the high-NO-coverage surface (2.02 eV) compared to the clean surface (0.79 eV). The transition states on the two surfaces are the same, with the O and N atoms at neighboring bridge sites (Figure 4). On the high-coverage surface, at the transition state, the NO spectators are at neighboring top sites.

NO* + H* → HNO* + *. The formation of HNO* from NO* and H* is endothermic on the low-coverage surface (ΔE = 0.40 eV) and exothermic (ΔE = −0.51 eV) on the high-coverage surface. The activation energy barrier is significantly lower than the direct NO dissociation activation energy barrier on both the low-coverage and high-coverage surfaces, suggesting that a H-assisted pathway is likely on Pt(111) regardless of the NO surface coverage. The barrier for this hydrogenation step is 0.65 eV lower on the high-coverage surface (E_A = 0.36 eV) than on the low-coverage surface (E_A = 1.01 eV). On clean Pt(111) and high-NO-coverage Pt(111), the N−H bond in HNO* at the transition state lies above a bridge site (Figure 4).

NO* + H* → NOH* + *. Whereas NO* can alternatively be hydrogenated to form NOH* on the low-coverage surface, a direct pathway for this elementary step was not identified on the high-coverage surface. The activation energy barrier on clean Pt(111) (E_A = 1.32 eV) is higher by ~0.3 eV than the barrier to form HNO*. On the clean Pt(111) surface at the transition state, the adsorbed NO is at an fcc site tilted at an angle of 56° relative to the surface, and the H is at the edge of a Pt top site (Figure 4). The reaction energy on clean Pt(111) is 0.30 eV.

HNO* + NO* → NOH* + NO*. An alternative pathway to form NOH* on the high-coverage surface was investigated, via an elementary step involving the transfer of the hydrogen in HNO* to a neighboring NO*. This step has a low barrier of 0.21 eV, and HNO* and NOH* are approximately isoenergetic

Adsorbate	$\theta_{NO} = 0$ BE (eV) Site	$\theta_{NO} = 0.5$ BE (eV) Site; NO sites	Adsorbate	$\theta_{NO} = 0$ BE (eV) Site	$\theta_{NO} = 0.5$ BE (eV) Site; NO sites
NOH	-2.87 fcc	-2.00 fcc; hcp, top	NH$_3$	-0.66 top	-0.66 top; fcc, hcp
HNO	-1.75 br-top	-1.00 top; fcc, hcp	OH	-2.32 br	-2.06 top; fcc, hcp
HNOH	-1.69 br	-0.90 br; fcc, top	HNNO	-1.84 top-top	-0.26 top-top; fcc, top
N	-4.76 fcc	-3.55 fcc; hcp, top	NH$_2$OH	-0.94 top	-0.29 top; fcc, top
O	-4.31 fcc	-3.39 fcc; hcp, top	N$_2$H$_2$	-1.08 top	-0.68 top; fcc, hcp
H	-2.76 fcc	-2.44 br; fcc, top	ONNOH	-1.84 top-top	-0.39 top; fcc, hcp
NH	-4.13 fcc	-3.12 fcc; hcp, top	H$_2$O	-0.23 top	does not adsorb --
NH$_2$	-2.44 br	-1.82 br; fcc, top	N$_2$	-0.12 top	does not adsorb --

Figure 3. Binding energies, site preference, and top views of the minimum energy adsorption modes for the adsorbates on clean Pt(111) (low coverage) and on Pt(111) with 0.5 ML NO coadsorbed (high coverage). For the high NO coverage systems, the site of the adsorbate is reported first, followed by the preferred sites of the two coadsorbed NO molecules, all in the minimum energy configuration. All results are calculated in a 2 × 2 surface unit cell. Yellow, red, blue, and gray spheres represent H, O, N, and Pt, respectively.

(HNO* is more stable by 0.03 eV) on the high-coverage surface. At the transition state, the H−NO* is at a top site and the NO−H* is at an fcc site (Figure 4). The H atom is 1.32 Å from the N in the HNO* reactant and 1.23 Å from the O in the NOH* product.

NOH* + * → N* + OH*. The activation energy barrier for breaking the N−O bond in NOH* at high NO coverage is 1.81 eV, and the elementary step is endothermic with a reaction energy of 0.83 eV. On clean Pt(111), the activation energy barrier is lower (E_A = 1.07 eV), and the elementary step is exothermic with a reaction energy of −0.24 eV. At the transition state on the clean surface, the N is at an fcc site and the OH is at a neighboring top site. On the high-coverage surface, at the transition state, the N is at a bridge site and the OH is nearest to a top site directly across from the N (Figure 4).

HNO* + * → NH* + O*. The activation energy barrier for cleavage of the N−O bond in HNO* at high NO coverage is 2.26 eV and the reaction is endothermic with a reaction energy of 0.98 eV. On clean Pt(111), the activation energy barrier is 1.47 eV and the reaction is exothermic with a reaction energy of −0.19 eV. At the transition state on the clean surface, the O is nearest to a top site and the NH is nearest to a bridge site. On the high-coverage surface, the transition state is similar to that found for direct NO dissociation: the O and the NH are located in neighboring bridge sites (Figure 4).

HNO* + H* → HNOH* + *. At high and low NO coverage, the activation energy barrier for adding H* to HNO* is lower than the respective barriers for breaking the N−O bond in HNO*. In the presence of 0.5 ML of spectator NO, the activation energy barrier is 0.43 eV, and on the clean Pt(111) surface, the barrier is 0.36 eV. This elementary step is exothermic on the high- and low-coverage surfaces, with a reaction energy of −0.74 eV and −0.15 eV, respectively. The H atom is at a top site and the HNO is at a bridge site, tilted toward the H atom at an angle of 42.5° relative to the surface, at the transition state for this elementary step at low coverage. At high NO coverage, the H atom is also near a top site at the transition state, but the HNO is at a top site tilted at an angle of 30.3° relative to the surface (Figure 4).

NOH* + H* → HNOH* + *. On the low-coverage surface, the activation energy barrier for adding H* to NOH* (E_A = 1.09 eV) is approximately equal to the barrier for breaking the N−O bond in NOH* (E_A = 1.07 eV). In the case of the high-coverage surface, the activation energy barrier for adding H* to NOH* is lower (E_A = 1.24 eV) than the barrier for breaking the N−O bond in NOH* (E_A = 1.81 eV). At the transition state on the high-coverage surface, the NOH is oriented perpendicular to the surface nearest to an fcc site, and the H is nearest to the neighboring hcp site. At the transition state on the low-coverage surface, the NOH is at a bridge site, tilted at an angle of 49.4° relative to the surface, and the H is nearest to a top site across from the N end of the NOH (Figure 4). The elementary

Table 1. Activation Energy Barriers (E_A) and Reaction Energies (ΔE) for Elementary Steps on Clean Pt(111) (Low Coverage) and on Pt(111) with 0.5 ML NO Coadsorbates (High Coverage)^a

elementary step	low coverage		high coverage	
	E_A (eV)	ΔE (eV)	E_A (eV)	ΔE (eV)
NO* + * → N* + O*	2.32	0.79	3.52	2.02
NO* + H* → HNO* + *	1.01	0.40	0.36	−0.51
NO* + H* → NOH* + *	1.32	0.30	--	--
NOH* + * → N* + OH*	1.07	−0.24	1.81	0.83
HNO* + * → O* + NH*	1.47	−0.19	2.26	0.98
HNO* + NO* → NOH* + NO*	NS	NS	0.21	0.03
NOH* + H* → HNOH* + *	1.09	−0.02	1.24	−0.86
HNO* + H* → HNOH* + *	0.36	−0.15	0.43	−0.74
HNOH* + * → NH* + OH*	0.70	−0.83	1.67	0.09
HNOH* → N* + H₂O	--	--	1.36	−0.67
HNOH* + H* → NH* + H₂O + *	NS	NS	0.69	−1.52
N* + N* → N₂* + *	1.55	−1.94	1.60	−2.28
NO* + N* → N₂O + 2*	1.18	0.17	0.07	−2.50
N* + H* → NH* + *	0.80	−0.54	0.54	−1.32
NH* + H* → NH₂* + *	1.27	−0.09	0.95	−0.88
NH₂* + H* → NH₃* + *	0.54	−0.63	0.31	−1.98
O* + H* → OH* + *	0.91	−0.17	0.22	−1.71
OH* + H* → H₂O* + *	0.17	−0.73	0.15	−1.50
H₂ + 2* → H* + H*	0.00	−0.87	0.65	0.08
HNOH* + H* → NH₂OH* + *	NS	NS	0.65	−0.93
NO* + NH* → HNNO* + *	1.09	0.03	0.69	−0.90
HNNO* → N₂O + H*	1.46	0.48	0.72	−0.81
HNNO* + NO* → NOH* + N₂O + *	NS	NS	0.61	0.60
NH* + NO* → N* + HNO*	NS	NS	0.62	0.62
2NH* → H₂N₂* + *	NS	NS	2.83	−0.46
N₂O* + * → N₂* + O*	0.61	−1.43	--	--
NO* + NOH* → ONNOH* + *	0.98	0.16	NS	NS

^{a}"NS" indicates an elementary step that was not studied on the listed surface, and "--" indicates a step which has been studied; however, a direct path for the elementary step was not found on the listed surface.

step is approximately thermoneutral on the low-coverage surface ($\Delta E = -0.02$ eV) and exothermic ($\Delta E = -0.86$ eV) on the high-coverage surface.

HNOH* + * → NH* + OH*. The activation energy for N–O bond breaking in HNOH* at low coverage is 0.70 eV, and the reaction is exothermic with a reaction energy of −0.83 eV. On the high-coverage surface, the activation energy barrier is higher ($E_A = 1.67$ eV), and the elementary step is slightly endothermic ($\Delta E = 0.09$ eV). At the transition state at both low and high NO coverage, the OH is nearest to a top site, and the NH is nearest to a bridge site (Figure 4). The N–O distance at the transition state is the same at high and low coverage: 1.84 Å. On the high-coverage surface at the transition state, the OH is approximately 0.35 Å further above the top site, compared with the low-coverage transition state.

HNOH* → N* + H₂O$_{(g)}$. The elementary step HNOH* → N* + H₂O$_{(g)}$ is a concerted step involving N–O and N–H bond cleavage and O–H bond formation. This step does not occur directly on the low-coverage surface. On the high-coverage surface, this elementary step is exothermic with a reaction energy of −0.67 eV, and the activation energy barrier is 1.36 eV. At the transition state, the N–O bond distance is 2.04 Å, and the OH is rotated approximately 90° relative to the orientation of the OH in HNOH* (Figure 4).

HNOH* + H* → NH* + H₂O$_{(g)}$ + *. The elementary step HNOH* + H* → NH* + H₂O$_{(g)}$ + * is a concerted step and involves both N–O bond cleavage and O–H bond formation. This step was not studied on the low-coverage surface, because

it is unlikely that it would occur directly. On the high-coverage surface, this elementary step is exothermic with a reaction energy of −1.52 eV, and the activation energy barrier is 0.69 eV. At the transition state, the N–O bond distance is 1.52 Å (Figure 4).

2N* → N₂* + *. The activation energy barriers for N₂ formation from atomic nitrogen are high, and this step is exothermic on the high-coverage ($E_A = 1.60$ eV, $\Delta E = -2.28$ eV) and low-coverage ($E_A = 1.55$ eV, $\Delta E = -1.94$ eV) surfaces. The transition states are similar on both surfaces with the N atoms in neighboring bridge sites (Figure 4).

NO* + N* → N₂O$_{(g)}$ + 2*. N₂O formation via NO* + N* → N₂O$_{(g)}$ + 2* has a significantly higher barrier on the low-coverage ($E_A = 1.18$ eV) surface than on the high-coverage ($E_A = 0.07$ eV) surface. This step is slightly endothermic ($\Delta E = 0.17$ eV) on the low-coverage surface and highly exothermic ($\Delta E = -2.50$ eV) on the high-coverage surface. On the high-coverage surface, at the transition state, N is at an fcc site and NO is at a bridge site with an N–N distance of 2.28 Å. At the transition state on the low-coverage surface, the N–N distance of 1.94 Å is shorter. At the transition state on the low-coverage surface, the N atom is at an hcp site and the NO is nearest to a top site (Figure 4).

NO* + NH* → HNNO* + *. The formation of HNNO*, via N–N bond formation between NH* and NO*, has an activation energy barrier of 0.69 eV on the high-NO-coverage Pt(111) surface and is exothermic with a reaction energy of −0.90 eV. The activation energy barrier on clean Pt(111) is

Elementary Step	TS $\theta_{NO}=0$	TS $\theta_{NO}=0.5$	Elementary Step	TS $\theta_{NO}=0$	TS $\theta_{NO}=0.5$	Elementary Step	TS $\theta_{NO}=0$	TS $\theta_{NO}=0.5$
$H_2 + 2^* \rightarrow 2H^*$	$E_A = 0$ eV		$HNOH^* + ^* \rightarrow NH^* + OH^*$			$HNOH^* + H^* \rightarrow NH^* + H_2O_{(g)} + ^*$	NS	
$NO^* + ^* \rightarrow N^* + O^*$			$HNOH^* \rightarrow N^* + H_2O_{(g)}$	--		$HNOH^* + H^* \rightarrow NH_2OH^* + ^*$	NS	
$NO^* + H^* \rightarrow HNO^* + ^*$			$2N^* \rightarrow N_2^* + ^*$			$NO^* + NH^* \rightarrow HNNO^* + ^*$		
$NO^* + H^* \rightarrow NOH^* + ^*$		--	$NO^* + N^* \rightarrow N_2O_{(g)} + 2^*$			$HNNO^* \rightarrow N_2O_{(g)} + H^*$		
$HNO^* + ^* \rightarrow NH^* + O^*$			$N^* + H^* \rightarrow NH^* + ^*$			$HNNO^* + NO^* \rightarrow NOH^* + N_2O_{(g)} + ^*$	NS	
$NOH^* + ^* \rightarrow N^* + OH^*$			$NH^* + H^* \rightarrow NH_2^* + ^*$			$NH^* + NO^* \rightarrow N^* + HNO^*$	NS	
$HNO^* \rightarrow NOH^*$	NS		$NH_2^* + H^* \rightarrow NH_3^* + ^*$			$2NH^* \rightarrow N_2H_2^* + ^*$	NS	
$HNO^* + H^* \rightarrow HNOH^* + ^*$			$O^* + H^* \rightarrow OH^* + ^*$			$N_2O^* + ^* \rightarrow N_2^* + O^*$		--
$NOH^* + H^* \rightarrow HNOH^* + ^*$			$OH^* + H^* \rightarrow H_2O^* + ^*$			$NO^* + NOH^* \rightarrow ONNOH^* + ^*$		NS

Figure 4. Transition state (TS) configurations of elementary steps on clean Pt(111) (low coverage) and on Pt(111) with 0.5 ML NO coadsorbates (high coverage). "NS" indicates an elementary step that was not studied on the listed surface, and "—" indicates a step for which a direct path was not found on the listed surface. Yellow, red, blue, and gray spheres represent H, O, N, and Pt, respectively.

higher, and the reaction step is thermoneutral ($E_A = 1.09$ eV, $\Delta E = 0.03$ eV). At the transition state (Figure 4) on the high-coverage surface, the NH and the NO are at neighboring bridge sites, and the N–N bond distance is 1.55 Å. On the clean surface at the transition state, the NH is at a bridge site, and the NO is nearest to a top site. The N–N bond distance is 1.83 Å.

$HNNO^* \rightarrow N_2O_{(g)} + H^*$. On the high-NO-coverage Pt(111) surface, the activation energy barrier for breaking the N–H bond in HNNO* to produce N_2O in the gas phase is 0.72 eV. On clean Pt(111), the barrier is 1.46 eV. This step is exothermic on the high-coverage surface ($\Delta E = -0.81$ eV) and endothermic on clean Pt(111) ($\Delta E = 0.48$ eV). The transition state is similar on the two surfaces (Figure 4). The N–N–O lies approximately parallel to the surface above a bridge site, with the O end tilted away from the surface, and the H is nearest to a top site. The N–H bond distance is 1.04 and 1.30 Å, on the high-NO-coverage surface and on clean Pt(111), respectively. The H atom cannot be seen in Figure 4 because it lies directly below the N end.

NH_3 Formation. The three hydrogen addition steps required to form NH_3 through hydrogenation of an adsorbed N atom have lower activation energy barriers and are more exothermic on the high-coverage surface compared to the low-coverage surface. The first hydrogenation step, to form NH* from N*, has a barrier of 0.80 eV and a reaction energy of -0.54 eV on the low-coverage surface. On the high-coverage surface, the activation energy barrier is 0.54 eV, and the reaction energy is -1.32 eV. The transition states are similar on both surfaces: the N atom is at an fcc site and the H atom is nearest to a top site (Figure 4). On both surfaces, the addition of the second H atom to form NH_2^* from NH* has the highest barrier of the three hydrogenation steps. The activation energy barrier for $NH^* + H^* \rightarrow NH_2^* + ^*$ is 1.27 eV at low coverage

and 0.95 eV at high NO coverage. This elementary step is exothermic on both surfaces with a reaction energy of -0.09 eV at low coverage and -0.88 eV at high NO coverage. At the transition state on the high- and low-coverage surfaces, the H atom is nearest to a top site. On the low-coverage surface, the NH is at a bridge site at the transition state, whereas on the high-NO-coverage surface at the transition state, the NH is at an fcc site (Figure 4). The third hydrogenation step, leading to adsorbed NH_3, has an activation energy barrier of 0.54 and 0.31 eV and a reaction energy of -0.63 eV and -1.98 eV on the low-coverage and high-NO-coverage surfaces, respectively. The transition state for this third hydrogenation step is similar on the two surfaces, with the NH_2 and the H atom located nearest to neighboring top sites (Figure 4).

H_2O Formation. The activation energy barrier for hydrogenation of O* to form OH* is 0.91 eV on the clean Pt(111) and 0.22 eV on the high-NO-coverage Pt(111) surface. The elementary step is more exothermic on the high-coverage ($\Delta E = -1.71$ eV) surface compared to the low-coverage ($\Delta E = -0.17$ eV) surface. At the transition state on the low-coverage surface, the O is at a bridge site, and the H is at a top site. On the high-coverage surface at the transition state, both O and H are at neighboring bridge sites (Figure 4).

The formation of H_2O from OH* has a similar activation energy barrier on the two surfaces: 0.17 eV at low coverage and 0.15 eV at high NO coverage. This elementary step is more exothermic on the high-coverage surface, with a reaction energy of -1.50 eV compared to a reaction energy of -0.73 eV on the low-coverage surface.

In general, the activation energy barriers for the bond-making steps decrease at higher NO coverage, and the activation energy barriers for the bond-breaking steps increase with increasing coverage. This general trend is observed because a significant

component of the activation energy barrier is related to the binding energy of reactants and products of elementary steps. For instance, on the high-coverage surface, the individual reactants of a bond-making step are bound more weakly compared to adsorption on the clean surface. As a result, it is easier for them to reach the transition state for the bond-making step, relative to the clean surface, which gives rise to a smaller barrier for a bond-making step on the high-coverage surface. Analogous arguments explain the general trend observed for the bond-breaking steps: a smaller barrier on the clean surface. The hydrogenation of NOH* and HNO*, and the formation of N_2 via the combination of two N* species $(2N^* \rightarrow N_2^* + ^*)$ do not follow this general principle; these bond-making steps have higher activation energy barriers at the higher NO coverage. However, the difference between the calculated activation energy barrier at high and low coverage is less than 0.15 eV for all three of these steps. The bond-breaking step HNNO* $\rightarrow$ N_2O + H* does not follow the general trend: the activation energy barrier is lower on the high-coverage surface. Because this step produces N_2O in the gas phase, it significantly reduces the repulsive interactions on the high-coverage surface and is therefore exothermic on the high-coverage surface. In contrast, it is an endothermic step on the low-coverage surface.

Maximum Rate Analysis. From the elementary steps outlined above, multiple pathways are possible for cleavage of the N−O bond,[35] shown schematically in Figure 5. The N−O
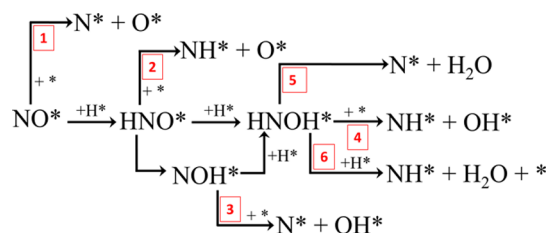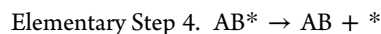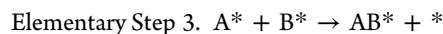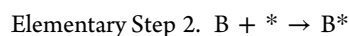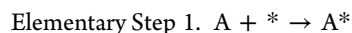

Figure 5. Reaction mechanisms for N−O bond activation in NO reduction by H_2. Labels with red numbers correspond to mechanisms in Table 2. DFT calculations showed that NO* + H* $\rightarrow$ NOH* + * does not occur as an elementary step on Pt(111) at high NO coverage. Mechanisms 4, 5, and 6 could all occur via step (i) HNO* + H* $\rightarrow$ HNOH* + * or step (ii) HNO* + H* $\rightarrow$ NOH* + H* $\rightarrow$ HNOH* + *. Because the maximum rates for the elementary steps in (i) are larger than those in (ii), we only consider path (i) in the analysis of mechanisms 4−6, although we do not exclude the possibility that NOH* could participate.

bond activation mechanisms considered all lead to either N* or NH*. In the case of NH*, adsorbed atomic nitrogen could then be formed by N−H dissociation such that all pathways lead to N_2O via N* + NO* $\rightarrow$ N_2O + 2*. The most commonly utilized and simplest procedure for assessing which of multiple competing reaction pathways may carry the flux in an overall reaction involves identifying the minimum energy pathway by plotting the energy or enthalpy versus the reaction coordinate for the various pathways. This approach, while informative, fails to consider potentially significant entropic effects. Therefore, a more detailed analysis involves constructing plots of the Gibbs free energy versus the reaction coordinate. Still, these plots of energy or Gibbs free energy versus reaction coordinate can be misleading, because the location of the highest transition state energy can depend on the order in which the steps are plotted. For example, by changing the order of the elementary steps,

specifically the adsorption steps, in direct NO dissociation (mechanism 1) on clean Pt(111), the location of the maximum transition state energy in the Gibbs free energy surface can change (see Figure 6). For this reason, the most rigorous procedure to predict the reaction flux through a specific pathway is generation of a full microkinetic model,[11,12] which requires significant time and effort, particularly for reactions with multiple products and many possible pathways. Accordingly, prior to conducting detailed microkinetic analyses, we suggest here a maximum rate analysis to probe the viability of various possible reaction pathways. This systematic analysis alleviates the issue with the ordering of elementary steps in kinetic analyses using plots of energy versus reaction coordinate, because all transition state energies are calculated relative to gas-phase reactants and products. In addition, the maximum rate analysis, outlined below, can be particularly useful for reducing the complexity of a subsequent microkinetic model by justifying the elimination of those elementary steps with very slow maximum rates.

To determine the most likely pathways via the maximum rate analysis, we first calculate the maximum rate of each elementary step in each mechanism based on the assumption that this step is the rate-determining step and that all other elementary steps in the mechanism are equilibrated. The rate of an elementary step involving a vacant site term is maximized when there is no site-blocking and therefore θ_*, the fraction of vacant surface sites, is equal to one. Partial pressures of gas-phase reactants and products and the reaction temperature are set on the basis of the conditions of experimental studies. In this case, we use a typical set of experimental conditions for this reaction: temperature of 400 K and NO, H_2, N_2O, and H_2O partial pressures of 0.005, 0.050, 0.0002, and 0.0002 atm, respectively. Once the maximum rate of each elementary step has been calculated, the values for the slowest maximum rate in the competing mechanisms are compared and discussed. The most likely reaction mechanisms are identified as those mechanisms with the largest calculated maximum rate for the slowest elementary step in the mechanism.

To illustrate the maximum rate analysis procedure, we derive the maximum rate equation for elementary steps in two example reaction mechanisms of differing complexity. We start with a simple reaction mechanism for the overall reaction A + B $\rightarrow$ AB:

Elementary Step 1. A + * $\rightarrow$ A*

Elementary Step 2. B + * $\rightarrow$ B*

Elementary Step 3. A* + B* $\rightarrow$ AB* + *

Elementary Step 4. AB* $\rightarrow$ AB + *

We now calculate the maximum rate of any individual step, assuming all of the other steps are in equilibrium. Based on transition state theory, the rate of reaction 1, (r_1), in units of molecules per area per time, is equal to the concentration of the activated complex times a frequency factor equal to k_BT/h, where k_B is the Boltzmann constant, T is the temperature and h is Planck's constant. For surface reactions, r_1 can be written as a turnover frequency, in units of s^{-1}, by dividing by the total concentration of surface sites, S_0, in units of sites per area.

$$r_1 = \frac{k_B T}{h S_0}[A^{*\ddagger}]$$
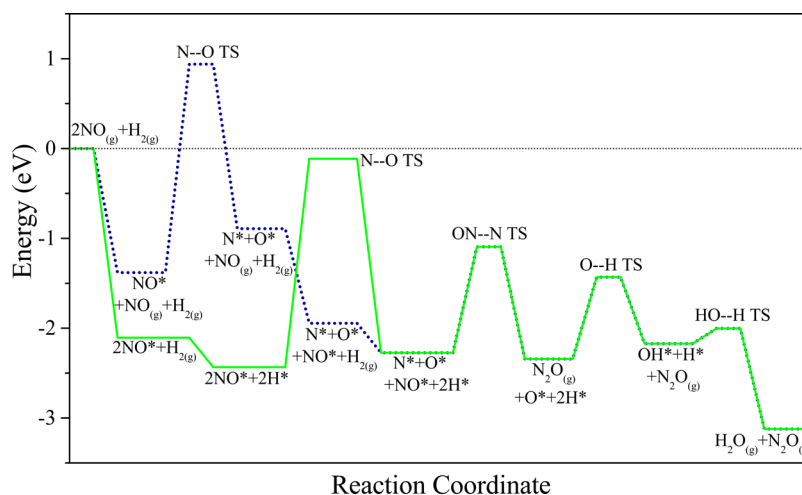
Figure 6. Free energy surface for direct NO dissociation (mechanism 1) on clean Pt(111). The solid green line shows the PES constructed with all adsorption steps occurring along the reaction coordinate before the N−O bond-breaking step. The dotted blue line shows the PES constructed with the second NO adsorption step and H_2 dissociative adsorption occurring in the reaction coordinate after N−O bond-breaking.

The equilibrium constant, $K_1^{\ddagger}$, for production of the activated complex $A^{*\ddagger}$ from gas-phase A is

$$K_1^{\ddagger} = e^{-\Delta G_1^{\ddagger}/k_B T} = \frac{\alpha_{A^{*\ddagger}}}{\alpha_A \alpha_*}$$

where $\Delta G_1^{\ddagger}$ is the Gibbs Free energy change for formation of the activated complex from gas-phase A and α_i is the activity of species i. The activity of gas-phase species A is the partial pressure of A, P_A, divided by the standard state pressure, P^0, of 1 atm. The activity of a surface adsorbate is the concentration of the adsorbate, in units of molecules per area, divided by the standard state, which is the total concentration of surface sites (S_0). This normalization gives the fractional surface coverage of surface adsorbate i, θ_i. Likewise, the activity term for vacant sites is the fractional coverage of empty sites, θ_*. $K_1^{\ddagger}$ can now be written as

$$K_1^{\ddagger} = e^{-\Delta G_1^{\ddagger}/k_B T} = \frac{\frac{[A^{*\ddagger}]}{S_0}}{\frac{P_A[*]}{P^0 S_0}} = \frac{\theta_{A^{*\ddagger}}}{p_A \theta_*}$$

where p_i is the partial pressure of i divided by the standard state pressure. The Gibbs free energy change of step j is calculated from the change in enthalpy and entropy

$$\Delta G_j^{\ddagger} = \Delta H_j^{\ddagger} - T * \Delta S_j^{\ddagger}$$

The enthalpy and entropy of gas-phase species are found from the energy and vibrational frequency calculations and their temperature dependence is described using the Shomate equation. The procedure for calculating the thermodynamic parameters for gas-phase species has been described in detail elsewhere.[12,36] For adsorbed species, the enthalpy is calculated by adding the DFT-derived binding energy to the enthalpy of the species in the gas phase. The entropy of an adsorbate is approximated as its local entropy, where the local entropy is the entropy of the species in the gas phase minus its 3D translational entropy. This choice for the entropy approximation is adequate due to the approximate nature of the maximum rate analysis, whereas more rigorous methods based on DFT calculations of the frustrated vibrational and rotational modes of adsorbed species could be used later, in a full microkinetic model. The entropy at the transition state is set

equal to the final state entropy for bond-making steps and the initial state entropy for bond-breaking steps. The enthalpy at the transition state is equal to the initial state enthalpy plus the DFT-calculated activation energy barrier.

The reaction rate is maximized when there is no site-blocking, such that θ_* is equal to unity. Thus, the maximum value of r_1, $r_{1,max}$, is given by

$$r_{1,max} = \frac{k_B T}{h} e^{-\Delta G_1^{\ddagger}/k_B T} p_A$$

Similar analysis leads to the analogous expression for $r_{2,max}$.

$$r_{2,max} = \frac{k_B T}{h} e^{-\Delta G_2^{\ddagger}/k_B T} p_B$$

The rate of reaction 3, r_3, and the equilibrium constant for production of the activated complex $AB^{**\ddagger}$ from adsorbed A and B are

$$r_3 = \frac{k_B T}{h} \theta_{AB^{**\ddagger}} \qquad K_3^{\ddagger} = e^{-\Delta G_3^{\ddagger}/k_B T} = \frac{\theta_{AB^{**\ddagger}}}{\theta_A \theta_B}$$

To derive the rate expression for step 3 in terms of gas-phase reactants and products, we use the equilibrium constant equations for elementary steps 1 and 2, because these steps are assumed to be equilibrated, to express θ_A and θ_B in terms of p_A and p_B.

$$K_3^{\ddagger} = e^{-\Delta G_3^{\ddagger}/k_B T} = \frac{\theta_{AB^{**\ddagger}}}{e^{-\Delta G_1/k_B T} e^{-\Delta G_2/k_B T} p_A p_B \theta_*^2}$$

The expression for $r_{3,max}$ thus becomes

$$r_{3,max} = \frac{k_B T}{h} e^{(-\Delta G_3^{\ddagger} - \Delta G_1 - \Delta G_2)/k_B T} p_A p_B$$

Importantly, this expression for $r_{3,max}$ could alternatively be derived by adding the elementary steps to generate an overall reaction, 3^{sum}, for the formation of the activated complex $AB^{**\ddagger}$ directly from gas-phase A and B.
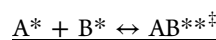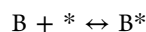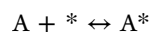
$$A + * \leftrightarrow A^*$$

$$B + * \leftrightarrow B^*$$

$$\underline{A^* + B^* \leftrightarrow AB^{**\ddagger}}$$

Table 2. Maximum Rates of Elementary Steps for N$_2$O Production in NO Reduction by H$_2$[a]

		mechanism 1		
step		overall reaction	rate constant	r_{max}
(1)	NO + * → NO*	NO + * ↔ NO*‡	$K_1^{\ddagger}$	5×10^{10}
(2)	H$_2$ + 2* → 2H*	H$_2$ + 2* ↔ 2H*‡	$K_2^{\ddagger}$	3×10^3
(3)	**NO* + * → N* + O***	**NO + 2* ↔ [N* + O*]‡**	**$K_3^{\ddagger}K_1$**	**2×10^{-29}**
(4)	N* + NO* → N$_2$O + 2*	2NO + H$_2$ + 2* ↔ [N$_2$O + 2*]‡ + H$_2$O	$K_4^{\ddagger}K_1^2K_2K_3K_5K_6$	8×10^{32}
(5)	O* + H* → OH* + *	2NO + 1/2H$_2$ + 2* ↔ [OH**]‡ + N$_2$O	$K_5^{\ddagger}K_1^2K_2^{1/2}K_3K_4$	8×10^{27}
(6)	OH* + H* → H$_2$O + 2*	2NO + H$_2$ + 2* ↔ [H$_2$O + 2*]‡ + N$_2$O	$K_6^{\ddagger}K_1^2K_2K_3K_4K_5$	7×10^{43}
min(r_{max})				**2×10^{-29}**
		mechanism 2		
step		overall reaction	rate constant	r_{max}
(1)	NO + * → NO*	NO + * ↔ NO*‡	$K_1^{\ddagger}$	5×10^{10}
(2)	H$_2$ + 2* → 2H*	H$_2$ + 2* ↔ 2H*‡	$K_2^{\ddagger}$	3×10^3
(3)	NO* + H* → HNO* + *	NO + 1/2H$_2$ + 2* ↔ [HNO**]‡	$K_3^{\ddagger}K_1K_2^{1/2}$	6×10^9
(4)	**HNO* + * → NH* + O***	**NO + 1/2H$_2$ + 2* ↔ [NH* + O*]‡**	**$K_4^{\ddagger}K_1K_2^{1/2}K_3$**	**5×10^{-16}**
(5)	NH* + * → N* + H*	NO + 3/2H$_2$ + 2* ↔ [N* + H*]‡ + H$_2$O	$K_5^{\ddagger}K_1K_2^{3/2}K_3K_4K_7K_8$	2×10^{22}
(6)	N* + NO* → N$_2$O + 2*	2NO + H$_2$ + 2* ↔ [N$_2$O + 2*]‡ + H$_2$O	$K_6^{\ddagger}K_1^2K_2K_3K_4K_5K_7K_8$	8×10^{32}
(7)	O* + H* → OH* + *	2NO + 1/2H$_2$ + 2* ↔ [OH**]‡ + N$_2$O	$K_7^{\ddagger}K_1^2K_2^{1/2}K_3K_4K_5K_6K_8$	8×10^{27}
(8)	OH* + H* → H$_2$O + 2*	2NO + H$_2$ + 2* ↔ [H$_2$O + 2*]‡ + N$_2$O	$K_8^{\ddagger}K_1^2K_2K_3K_4K_5K_6K_8$	7×10^{43}
min(r_{max})				**5×10^{-16}**
		mechanism 3		
step		overall reaction	rate constant	r_{max}
(1)	NO + * → NO*	NO + * ↔ NO*‡	$K_1^{\ddagger}$	5×10^{10}
(2)	H$_2$ + 2* → 2H*	H$_2$ + 2* ↔ 2H*‡	$K_2^{\ddagger}$	3×10^3
(3)	NO* + H* → HNO* + *	NO + 1/2H$_2$ + 2* ↔ [HNO**]‡	$K_3^{\ddagger}K_1K_2^{1/2}$	6×10^9
(4)	HNO* → NOH*	NO + 1/2H$_2$ + * ↔ [NOH*]‡	$K_4^{\ddagger}K_1K_2^{1/2}K_3$	3×10^{10}
(5)	**NOH* + * → N* + OH***	**NO + 1/2H$_2$ + 2* ↔ [N* + OH*]‡**	**$K_5^{\ddagger}K_1K_2^{1/2}K_3K_4$**	**1×10^{-10}**
(6)	N* + NO* → N$_2$O + 2*	2NO + H$_2$ + 2* ↔ [N$_2$O + 2*]‡ + H$_2$O	$K_6^{\ddagger}K_1^2K_2K_3K_4K_5K_7$	8×10^{32}
(7)	OH* + H* → H$_2$O + 2*	2NO + H$_2$ + 2* ↔ [H$_2$O + 2*]‡ + N$_2$O	$K_7^{\ddagger}K_1^2K_2K_3K_4K_5K_6$	7×10^{43}
min(r_{max})				**1×10^{-10}**
		mechanism 4		
step		overall reaction	rate constant	r_{max}
(1)	NO + * → NO*	NO + * ↔ NO*‡	$K_1^{\ddagger}$	5×10^{10}
(2)	H$_2$ + 2* → 2H*	H$_2$ + 2* ↔ 2H*‡	$K_2^{\ddagger}$	3×10^3
(3)	NO* + H* → HNO* + *	NO + 1/2H$_2$ + 2* ↔ [HNO**]‡	$K_3^{\ddagger}K_1K_2^{1/2}$	6×10^9
(4)	HNO* + H* → HNOH* + *	NO + H$_2$ + 2* ↔ [HNOH**]‡	$K_4^{\ddagger}K_1K_2K_3$	5×10^5
(5)	**HNOH* + * → NH* + OH***	**NO + H$_2$ + 2* ↔ [NH* + OH*]‡**	**$K_5^{\ddagger}K_1K_2K_3K_4$**	**5×10^{-7}**
(6)	NH* + * → N* + H*	NO + 3/2H$_2$ + 2* ↔ [N* + H*]‡ + H$_2$O	$K_6^{\ddagger}K_1K_2^{3/2}K_3K_4K_5K_8$	2×10^{22}
(7)	N* + NO* → N$_2$O + 2*	2NO + H$_2$ + 2* ↔ [N$_2$O + 2*]‡ + H$_2$O	$K_7^{\ddagger}K_1^2K_2K_3K_4K_5K_6K_8$	8×10^{32}
(8)	OH* + H* → H$_2$O + 2*	2NO + H$_2$ + 2* ↔ [H$_2$O + 2*]‡ + N$_2$O	$K_8^{\ddagger}K_1^2K_2K_3K_4K_5K_6K_7$	7×10^{43}
min(r_{max})				**5×10^{-7}**
		mechanism 5		
step		overall reaction	rate constant	r_{max}
(1)	NO + * → NO*	NO + * ↔ NO*‡	$K_1^{\ddagger}$	5×10^{10}
(2)	H$_2$ + 2* → 2H*	H$_2$ + 2* ↔ 2H*‡	$K_2^{\ddagger}$	3×10^3
(3)	NO* + H* → HNO* + *	NO + 1/2H$_2$ + 2* ↔ [HNO**]‡	$K_3^{\ddagger}K_1K_2^{1/2}$	5×10^9
(4)	HNO* + H* → HNOH* + *	NO + H$_2$ + 2* ↔ [HNOH**]‡	$K_4^{\ddagger}K_1K_2K_3$	5×10^5
(5)	**HNOH* → N* + H$_2$O**	**NO + H$_2$ + * ↔ [N* + H$_2$O]‡**	**$K_5^{\ddagger}K_1K_2K_3K_4$**	**4×10^{-3}**
(6)	N* + NO* → N$_2$O + 2*	2NO + H$_2$ + 2* ↔ [N$_2$O + 2*]‡ + H$_2$O	$K_6^{\ddagger}K_1^2K_2K_3K_4K_5$	6×10^{32}
min(r_{max})				**4×10^{-3}**
		mechanism 6		
step		overall reaction	rate constant	r_{max}
(1)	NO + * → NO*	NO + * ↔ NO*‡	$K_1^{\ddagger}$	5×10^{10}
(2)	**H$_2$ + 2* → 2H***	**H$_2$ + 2* ↔ 2H*‡**	**$K_2^{\ddagger}$**	**3×10^3**
(3)	NO* + H* → HNO* + *	NO + 1/2H$_2$ + 2* ↔ [HNO**]‡	$K_3^{\ddagger}K_1K_2^{1/2}$	5×10^9
(4)	HNO* + H* → HNOH* + *	NO + H$_2$ + 2* ↔ [HNOH**]‡	$K_4^{\ddagger}K_1K_2K_3$	5×10^5
(5)	HNOH* + H* → NH* + H$_2$O + *	NO + 3/2H$_2$ + 2* ↔ [NH* + H$_2$O*]‡	$K_5^{\ddagger}K_1K_2^{3/2}K_3K_4$	8×10^7
(6)	NH* + * → N* + H*	NO + 3/2H$_2$ + 2* ↔ [N* + H*]‡ + H$_2$O	$K_6^{\ddagger}K_1K_2^{3/2}K_3K_4K_5$	2×10^{22}
(7)	N* + NO* → N$_2$O + 2*	2NO + H$_2$ + 2* ↔ [N$_2$O + 2*]‡ + H$_2$O	$K_7^{\ddagger}K_1^2K_2K_3K_4K_5K_6$	6×10^{32}

Table 2. continued

mechanism 6			
step	overall reaction	rate constant	r_{max}
$\min(r_{max})$			$\mathbf{3 \times 10^3}$

[a]Maximum rates of elementary steps in competing reaction mechanisms, outlined in Figure 5, as calculated from DFT-derived data on Pt(111) with 0.5 ML NO spectators. Rates are calculated at a temperature of 400 K and NO, H_2, H_2O and N_2O partial pressures of 0.005, 0.050, 0.0002 and 0.0002 atm, respectively. In each mechanism the slowest step is indicated in bold face.

$$A + B + 2^* \leftrightarrow AB^{**\ddagger} \tag{3^{sum}}$$

The equilibrium constant for production of the activated complex $AB^{**\ddagger}$ from gas-phase A and B can then be used to derive an expression for the coverage of the activated complex $\theta_{AB^{**\ddagger}}$. The equilibrium constant is calculated as

$$K_{3,sum}^{\ddagger} = K_3^{\ddagger} K_1 K_2 = e^{-\Delta G_3^{\ddagger}/k_B T} e^{-\Delta G_1/k_B T} e^{-\Delta G_2/k_B T} = \frac{\theta_{AB^{**\ddagger}}}{p_A p_B \theta_*^2}$$

where K_1 and K_2 are the equilibrium constants for elementary step 1 and 2, respectively. We can then add the three free energy change terms to determine $\Delta G_{3,sum}^{\ddagger}$, the change in Gibbs free energy for the formation of the activated complex from gas-phase A and B. This lumping results in the elimination of all of the free energy terms for A* and B*.
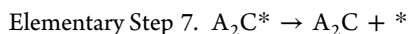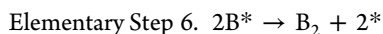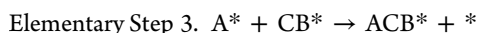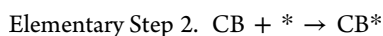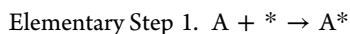
$$-\Delta G_{3,sum}^{\ddagger} = -\Delta G_3^{\ddagger} - \Delta G_1 - \Delta G_2$$
$$= -(G_{AB^{**\ddagger}} - G_{A^*} - G_{B^*}) - (G_{A^*} - G_A) - (G_{B^*} - G_B)$$
$$= -(G_{AB^{**\ddagger}} - G_A - G_B)$$

$$r_{3,max} = \frac{k_B T}{h} e^{-\Delta G_{3,sum}^{\ddagger}/k_B T} p_A p_B$$

Lastly, the maximum rate expression for elementary step 4 is

$$r_{4,max} = \frac{k_B T}{h} e^{-\Delta G_{4,sum}^{\ddagger}/k_B T} p_A p_B$$

The approach of adding all of the elementary steps to generate an overall equation involving only the activated complex in the assumed rate-determining step and gas-phase reactants and products is particularly useful when calculating maximum rates of elementary steps in more complicated reaction mechanisms. For example, below is one possible reaction mechanism for the overall reaction $4A + 2CB \rightarrow 2A_2C + B_2$.
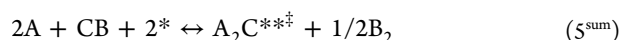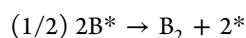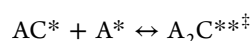
Elementary Step 1. $A + ^* \rightarrow A^*$

Elementary Step 2. $CB + ^* \rightarrow CB^*$

Elementary Step 3. $A^* + CB^* \rightarrow ACB^* + ^*$

Elementary Step 4. $ACB^* + ^* \rightarrow AC^* + B^*$

Elementary Step 5. $AC^* + A^* \rightarrow A_2C^* + ^*$

Elementary Step 6. $2B^* \rightarrow B_2 + 2^*$
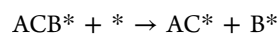
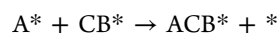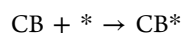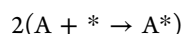Elementary Step 7. $A_2C^* \rightarrow A_2C + ^*$

For this example, we will only derive the equation for calculating the maximum rate of elementary step 5.

$$r_5 = \frac{k_B T}{h S_0} [A_2C^{**\ddagger}]$$

Assuming all other reactions are equilibrated and step 5 is rate-determining, the following elementary steps can be added to express the overall reaction for forming the activated complex $A_2C^{**\ddagger}$ from gas-phase reactants and products.

$$2(A + ^* \rightarrow A^*)$$

$$CB + ^* \rightarrow CB^*$$

$$A^* + CB^* \rightarrow ACB^* + ^*$$

$$ACB^* + ^* \rightarrow AC^* + B^*$$

$$AC^* + A^* \leftrightarrow A_2C^{**\ddagger}$$

$$\underline{(1/2)\ 2B^* \rightarrow B_2 + 2^*}$$

$$2A + CB + 2^* \leftrightarrow A_2C^{**\ddagger} + 1/2 B_2 \tag{5^{sum}}$$

The equilibrium constant is now written for the total reaction giving the production of the activated complex, $A_2C^{**\ddagger}$, from gas-phase A, CB and B_2, where all energy terms related to adsorbed intermediates cancel, leaving $\Delta G_{5,sum}^{\ddagger}$.

$$K_{5,sum}^{\ddagger} = K_5^{\ddagger} K_1^2 K_2 K_3 K_4 K_6^{1/2}$$
$$= e^{-\Delta G_5^{\ddagger}/k_B T} [e^{-\Delta G_1/k_B T}]^2 e^{-\Delta G_2/k_B T} e^{-\Delta G_3/k_B T} e^{-\Delta G_4/k_B T} [e^{-\Delta G_6/k_B T}]^{1/2}$$
$$= \frac{\theta_{A_2C^{**\ddagger}} p_{B_2}^{1/2}}{p_A^2 p_{CB} \theta_*^2}$$

$$\theta_{A_2C^{**\ddagger}} = e^{\frac{-\Delta G_{5,sum}^{\ddagger}}{k_B T}} \frac{p_A^2 p_{CB} \theta_*^2}{p_{B_2}^{1/2}}$$

Then we can use the expression for $\theta_{A_2C^{**\ddagger}}$ to calculate $r_{5,max}$.

$$r_{5,max} = \frac{k_B T}{h} e^{\frac{-\Delta G_{5,sum}^{\ddagger}}{k_B T}} \frac{p_A^2 p_{CB}}{p_{B_2}^{1/2}}$$

Once the maximum rates of all of the elementary steps in a reaction mechanism have been calculated, the minimum of these rates can be compared with the minimum rates of competing mechanisms to determine which mechanisms are most likely to carry the majority of the flux from reactants to products.

The maximum rate analysis was applied to determine the most likely mechanism(s) for N−O bond activation leading to formation of the major product observed experimentally, N_2O, in low-temperature NO reduction by H_2 on Pt catalysts.[7,8] The analysis was first conducted using the data from DFT calculations at high NO coverage (0.5 ML NO spectators), as this surface environment is expected to be more representative of realistic experimental conditions (see discussion earlier). The calculated maximum rates are shown in Table 2 for the individual elementary steps in all N−O activation mechanisms outlined schematically in Figure 5. Table 2 also shows the overall reaction for forming the activated complex in each elementary step from gas-phase reactants and products, and the resulting rate constant for the overall reaction. For each mechanism, the elementary step with the minimum value of its

maximum rate is reported in bold print below the mechanism in Table 2 and reported in the bar graph in Figure 7.
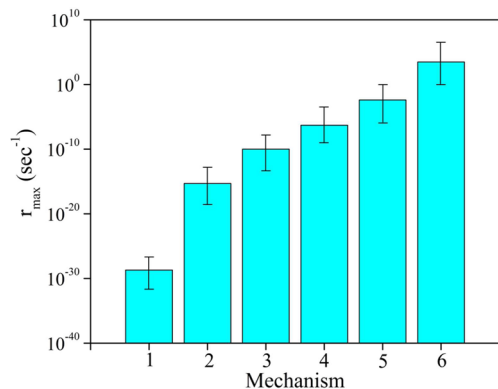
Figure 7. Maximum rates of the slowest step in each mechanism, shown in Figure 5, on Pt(111) with 0.5 ML NO spectators, calculated using DFT-derived data. The error bars are calculated by reducing (−) and increasing (+) the DFT-derived activation energy barriers of all steps in the mechanism by 0.2 eV. Rates are calculated at a temperature of 400 K and NO, H_2, H_2O and N_2O partial pressures of 0.005, 0.050, 0.0002, and 0.0002 atm, respectively.

To account for an estimated error in the DFT calculated activation energy barriers of ±0.2 eV, we calculated the upper and lower bounds of the maximum rates for the slowest elementary step in each mechanism, shown as error bars in Figure 7. For simplicity, we increased or decreased the activation energy barriers of all of the elementary steps so that the slowest step would not change throughout the uncertainty analysis. In mechanism 1 the slowest step is direct NO dissociation. The maximum rate for this step is low (2×10^{-29} s^{-1}), which is more than 12 orders of magnitude slower than the slowest step in all other mechanisms. Therefore, we eliminate the direct NO dissociation mechanism (mechanism 1) as a possible mechanism for the overall reaction. The slowest steps in mechanisms 2 and 3 are cleavage of the N−O bond in HNO* and NOH*, respectively. Based on the maximum rate calculations, these elementary steps are expected to be slower than the slowest steps in mechanisms 4−6. Additionally, the elementary step involving cleavage of the N−O bond in either HNO* or NOH* competes with the elementary steps involving hydrogenation of these intermediates leading to HNOH*, which occur in mechanisms 4−6. Comparison of the maximum rate for HNO* + * → NH* + O* ($r_{max} = 5 \times 10^{-16}$ s^{-1}) with the maximum rate for HNO* + H* → HNOH* + * ($r_{max} = 5 \times 10^{5}$ s^{-1}) suggests that the hydrogenation step should be more favorable, and thus mechanism 2 is unlikely to occur. This comparison is closer for NOH*, with maximum rates of 1×10^{-10} and 1×10^{-5} s^{-1} for NOH* + * → N* + OH* and NOH* + H* → HNOH* + *, respectively. However, on the basis of this difference of 5 orders of magnitude, we suggest that mechanism 3 is also an unlikely overall reaction mechanism.

Mechanisms 4, 5, and 6 can all occur via step (i) HNO* + H* → HNOH* + * or step (ii) HNO* + H* → NOH* + H* → HNOH* + *. Because the maximum rates for the elementary steps in (i) are larger than those in (ii), we only consider path (i) in the subsequent analysis of mechanisms 4−6, although we do not exclude the possibility that NOH* could participate. The maximum rate for the slowest step in

mechanism 4 (HNOH* + * → NH* + OH*) is 5×10^{-7} s^{-1}. The maximum rate for the slowest steps in mechanisms 5 (HNOH* → N* + $H_2O_{(g)}$, $r_{max} = 4 \times 10^{-3}$ s^{-1}) and 6 (H_2 + 2* → 2H*, $r_{max} = 3 \times 10^{3}$ s^{-1}) are similar, particularly when one accounts for the assumed error in the DFT-calculated activation energy barriers by comparing the upper and lower limits of the maximum rates. Importantly, the barrier for the slowest elementary step in mechanism 4 (HNOH* + * → NH* + OH*) was found to be highly dependent on the NO surface coverage. The barrier for the elementary step HNOH* + * → NH* + OH* increases from 0.70 eV at low coverage to 1.67 eV at high NO coverage. Furthermore, HNOH* is a large intermediate, which could result in an overestimation of the DFT-calculated high NO coverage barrier due to repulsive interactions. The concerted step HNOH* → N* + H_2O (mechanism 5) does not occur directly on the low-coverage surface. Likewise, the N−O bond breaking step required for mechanism 6, although it is not the slowest step in the mechanism, is also a concerted step that may not occur directly on the low-coverage surface. Additional theoretical studies of the coverage dependence of these steps as well as experimental studies of the NO surface coverage under realistic reaction conditions are necessary to conclusively state which of mechanisms 4−6 are most likely.

In summary, based on the maximum rate analysis, mechanisms 1, 2, and 3 are determined to be unlikely for the formation of N_2O in NO reduction by H_2 on Pt(111) with 0.5 ML NO spectators. Mechanism 1 occurs via direct NO dissociation, and mechanisms 2 and 3 occur via the addition of a single H atom to NO followed by N−O bond scission (in either HNO* or NOH*). The more energetically favorable pathways are suggested to be mechanisms that involve the addition of at least two hydrogen atoms prior to cleavage of the N−O bond. The results of this analysis suggest that HNO* and HNOH* are likely to be important reaction intermediates in NO reduction by H_2.

To further illustrate the importance of considering the most relevant surface coverage, we conducted maximum rate analyses using the DFT-derived data on clean Pt(111) and the same reaction conditions described above for high NO-coverage Pt(111). The maximum rate for the slowest step in mechanism 1, NO* + * → N* + O*, is 8×10^{-4} s^{-1}. For mechanism 2, the slowest step is N−O bond-breaking in HNO* (HNO* + * → NH* + O*, $r_{max} = 2 \times 10^{4}$ s^{-1}). For all other mechanisms considered on clean Pt(111) the slowest step is NO adsorption, which has a maximum rate of 5×10^{10} s^{-1}. The mechanisms involving concerted elementary steps for N−O bond-breaking in HNOH*, mechanisms 5 and 6, were not considered, because these steps are unlikely to occur directly at low NO coverage. Based on the maximum rates calculated, the direct NO dissociation mechanism (mechanism 1) and N−O bond scission via HNO* (mechanism 2) are unlikely to occur even at low NO coverage. Mechanism 3, however, which proceeds via NOH* dissociation, may be more competitive on clean Pt(111), compared to the high NO coverage system.

The results of our maximum rate analysis are insensitive to the specific conditions used. For example, the conclusions reported do not change if the partial pressures of gas-phase NO, H_2, H_2O, or N_2O used in the analysis are modified by 1 order of magnitude, because the conclusions are derived from a comparison of rates that differ by multiple orders of magnitude. The most sensitive parameter in this study is, in fact, the NO surface coverage utilized in the DFT calculations. Therefore,

one must ensure that the reaction conditions used in the maximum rate analysis are consistent with the surface coverages predicted by the DFT-derived phase diagram and that subsequent DFT calculations are performed on the appropriately modified (by adsorbates) clean surfaces.

We note that the elementary step for N_2O formation invoked throughout this study ($N^* + NO^* \rightarrow N_2O + 2^*$) may be overly simplistic. Because two of the three proposed reaction mechanisms (mechanisms 4 and 6) on high NO coverage Pt(111) require breaking the N–H bond in NH* to form N*, an elementary step with a high activation energy barrier ($E_A = 1.86$ eV), we investigated alternative routes leading to N_2O from NH*. One possible step is formation of an N–N bond with a neighboring NO* to produce the intermediate HNNO*, which may be particularly relevant because NO* is expected to be present at high coverage on Pt(111). The HNNO* can then undergo N–H bond scission to produce $N_2O_{(g)}$ and an adsorbed H atom. Interestingly, the calculated maximum rate for forming HNNO* (3×10^{35} s^{-1}) is more than 10 orders of magnitude greater than the maximum rate calculated for NH* $+ * \rightarrow N^* + H^*$ (2×10^{22} s^{-1}). A detailed analysis of product formation mechanisms through a DFT-based full microkinetic model and comparison with experimentally determined trends, will be necessary to determine the most likely steps involved in N_2O formation following the initial N–O bond scission. In addition, combining this theoretical study with experimental kinetics, including experiments probing the effect of the Pt particle size on the activity and selectivity of the reaction, will provide insight into the role of various types of surface sites in the reaction. The Pt(111) facet is the most stable and therefore most abundant facet of a Pt nanoparticle, but may not be the active site for the overall reaction. If a significant particle size effect is found, additional theoretical studies analogous to the one presented here should be conducted for a Pt slab with defect sites, such as steps and/or kinks. These sites are likely to display very different reaction energetics, compared to Pt(111) and consequently may provide alternative reaction pathways to those predicted here. Alternatively, these sites may be proven to be strongly poisoned by some reactive intermediates, thereby eliminating their effect on steady-state reaction kinetics. Detailed experimental studies of particle size effects will be essential in assessing the importance of under-coordinated Pt sites.

CONCLUSIONS

We showed that Pt(111) is mostly covered by adsorbed NO during NO reduction by H_2 at low temperatures (e.g., 400 K) and typical pressures. The high NO coverage destabilizes adsorbed intermediates. In general, high coverage causes the activation energy barriers for bond-breaking steps to increase and the activation energy barriers for bond-making steps to decrease, relative to the respective barriers on clean Pt(111). The activation energy barrier for N_2O formation from adsorbed N* and NO* decreases at high NO coverage, which is a possible explanation for the high N_2O selectivity observed experimentally at low temperatures.

A maximum rate analysis, a procedure for assessing the most likely reaction pathway(s) from DFT-derived kinetic and thermodynamic data, is performed to probe the reaction mechanisms leading to N_2O formation at low temperatures in NO reduction by H_2. The results of this analysis suggest that the addition of at least two H atoms is required prior to cleavage of the N–O bond. The intermediates HNO* and

HNOH* are likely important intermediates in the pathway to N_2O formation from NO and H_2 at low temperatures.

■ AUTHOR INFORMATION

Corresponding Authors
*E-mail: manos@engr.wisc.edu.
*E-mail: dumesic@engr.wisc.edu.

Notes
The authors declare no competing financial interest.

■ ACKNOWLEDGMENTS

■ REFERENCES

(1) Heck, R. M.; Farrauto, S. T.; Gulati, S. T. *Catalytic Air Pollution Control: Commercial Technology*; John Wiley & Sons: Hoboken, NJ, 2009; pp 403−439.
(2) Nieuwenhuys, B. E. *Adv. Catal.* **1999**, *44*, 259−328.
(3) Roy, S.; Hegde, M. S.; Madras, G. *Appl. Energy* **2009**, *86*, 2283−2297.
(4) Kobylinski, T. P.; Taylor, B. W. *J. Catal.* **1974**, *33*, 376−384.
(5) Shustorovich, E.; Bell, A. T. *Surf. Sci.* **1993**, *289*, 127−138.
(6) Burch, R.; Shestov, A. A.; Sullivan, J. A. *J. Catal.* **1999**, *186*, 353−361.
(7) Stenger, H. G.; Hepburn, J. S. *Energy Fuels* **1987**, *1*, 412−416.
(8) Zhou, S.; Varughese, B.; Eichhorn, B.; Jackson, G.; McIlwrath, K. *Angew. Chem., Int. Ed.* **2005**, *44*, 4539−4543.
(9) Kumar, A.; Medhekar, V.; Harold, M. P.; Balakotaiah, V. *Appl. Catal., B* **2009**, *90*, 642−651.
(10) Hirano, H.; Yamada, T.; Tanaka, K. I.; Siera, J.; Cobden, P.; Nieuwenhuys, B. E. *Surf. Sci.* **1992**, *262*, 97−112.
(11) Dumesic, J. A.; Rudd, D. F.; Aparicio, L. M.; Rekoske, J. E.; Trevino, A. A. *The Microkinetics of Heterogeneous Catalysis*. American Chemical Society: Washington, DC, 1993; pp 23−53.
(12) Gokhale, A. A.; Kandoi, S.; Greeley, J. P.; Mavrikakis, M.; Dumesic, J. A. *Chem. Eng. Sci.* **2004**, *59*, 4679−4691.
(13) Kresse, G.; Furthmüller, J. *Phys. Rev. B* **1996**, *54*, 11169−11186.
(14) Kresse, G.; Furthmüller, J. *Comput. Mater. Sci.* **1996**, *6*, 15−50.
(15) Perdew, J. P.; Wang, Y. *Phys. Rev. B* **1992**, *45*, 13244−13249.
(16) Blochl, P. E. *Phys. Rev. B* **1994**, *50*, 17953−17979.
(17) Kresse, G.; Joubert, D. *Phys. Rev. B* **1999**, *59*, 1758−1775.
(18) Monkhorst, H. J.; Pack, J. D. *Phys. Rev. B* **1976**, *13*, 5188−5192.
(19) Bengtsson, L. *Phys. Rev. B* **1999**, *59*, 12301−12304.
(20) Neugebauer, J.; Scheffler, M. *Phys. Rev. B* **1992**, *46*, 16067−16080.
(21) CRC *Handbook of Chemistry and Physics*, 95th ed.; CRC Press: Boca Raton, FL, 2014; pp 4−150.

(22) Henkelman, G.; Uberuaga, B. P.; Jonsson, H. *J. Chem. Phys.* **2000**, *113*, 9901−9904.

(23) Henkelman, G.; Jonsson, H. *J. Chem. Phys.* **2000**, *113*, 9978−9985.

(24) Greeley, J.; Mavrikakis, M. *Surf. Sci.* **2003**, *540*, 215−229.

(25) Zhu, J. F.; Kinne, M.; Fuhrmann, T.; Denecke, R.; Steinrück, H. P. *Surf. Sci.* **2003**, *529*, 384−396.

(26) Ford, D. C.; Xu, Y.; Mavrikakis, M. *Surf. Sci.* **2005**, *587*, 159−174.

(27) Ge, Q.; King, D. A. *Chem. Phys. Lett.* **1998**, *285*, 15−20.

(28) Huang, X.; Mason, S. E. *Surf. Sci.* **2014**, *621*, 23−30.

(29) Wartnaby, C. E.; Stuck, A.; Yeo, Y. Y.; King, D. A. *J. Phys. Chem.* **1996**, *100*, 12483−12488.

(30) Zeng, Z.-H.; Da Silva, J. L. F.; Deng, H.-Q.; Li, W.-X. *Phys. Rev. B* **2009**, *79*, 205413.

(31) Goldsmith, B. R.; Sanderson, E. D.; Ouyang, R. H.; Li, W.-X. *J. Phys. Chem. C* **2014**, *118*, 9588−9597.

(32) Reuter, K.; Scheffler, M. *Phys. Rev. B* **2002**, *65*, 035406.

(33) Gorte, R. J.; Schmidt, L. D.; Gland, J. L. *Surf. Sci.* **1981**, *109*, 367−380.

(34) Campbell, C. T.; Ertl, G.; Segner, J. *Surf. Sci.* **1982**, *115*, 309−322.

(35) Because the elementary step involving N—O bond breaking in NH_2OH^* was not included in this study, NH_2OH^* was not included as a possible intermediate in N—O activation

(36) Grabow, L. C.; Mavrikakis, M. *ACS Catal.* **2011**, *1*, 365−384.